Meteoritics & Planetary Science 40, Nr 1, 123–138 (2005)
Abstract available online at http://meteoritics.org

Chondrule and metal grain size sorting from jet flows

Kurt LIFFMAN[1, 2]

[1]Thermal and Fluids Engineering, Commonwealth Scientific and Industrial Research Organization, Manufacturing and Infrastructure Technology, P.O. Box 56, Highett, Victoria 3190, Australia
[2]School of Mathematical Sciences, Monash University, Clayton, Victoria 3163, Australia
E-mail: kurt.liffman@csiro.au

(Received 2 October 2003; revision accepted 26 November 2004)

Abstract–We examine the size sorting of chondrules and metal grains within the context of the jet flow model for chondrule/CAI formation. In this model, chondrules, CAIs, AOAs, metal grains, and related components of meteorites are assumed to have formed in the outflow region of the innermost regions of the solar nebula and then were ejected, via the agency of a bipolar jet flow, to outer regions of the nebula. We wish to see if size sorting of chondrules and metal grains is a natural consequence of this model. To assist in this task, we used a multiprocessor system to undertake Monte Carlo simulations of the early solar nebula. The paths of a statistically significant number of chondrules and metal grains were analyzed as they were ejected from the outflow and travelled over or into the solar nebula. For statistical reasons, only distances ≤3 AU from the Sun were examined.

Our results suggest that size sorting can occur provided that the solar nebula jet flow had a relatively constant flow rate as function of time. A constant flow rate outflow produces size sorting, but it also produces a sharp size distribution of particles across the nebula and a metal-rich Fe/Si ratio. When the other extreme of a fully random flow rate was examined, it was found that size sorting was removed, and the initial material injected into the flow was simply spread over most of the the solar nebula. These results indicate that the outflow can act as a size and density classifier. By simply varying the flow rate, the outflow can produce different types of proto-meteorites from the same chondrule and metal grain feed stock.

As a consequence of these investigations, we observed that the number of particles that impact into the nebula drops off moderately rapidly as a function of distance r from the Sun. We also derive a corrected form of the Epstein stopping time.

INTRODUCTION

Ever since H. C. Sorby (1877) first put forward a model of chondrule formation, at least twenty different theories have been proposed to explain the formation of the components observed in primitive meteorites (Grossman 1988; Boss 1996). At present, the most popular chondrule formation theory is the "shock model" (Hood and Horanyi 1991, 1993; Boss and Graham 1993; Ruzmaikina and Ip 1996; Wood 1996; Weidenschilling et al. 1998; Hood 1998; Connolly and Love 1998; Ciesla and Hood 2002; Desch and Connolly 2002), in which it is assumed that chondrules and other components of primitive meteorites were formed via the agency of shock waves, usually at around 3 AU from the Sun.

In this paper, we investigate another popular model of chondrule formation. We assume that chondrules were formed in a bipolar jet flow that was produced by the interaction between primordial Sun and the inner edge of the solar nebula at the very earliest stages of the formation of the solar system.

In this jet model (Skinner 1990; Liffman 1992; Cameron 1994; Liffman and Brown 1995; Shu et al. 1996; Liffman and Brown 1996), chondrules and refractory inclusions were formed and ejected from the inner solar nebula by a bipolar jet flow. In principle, a portion of the ejected particles can then travel across the face of the nebula where the increase in the disk height allows some of the chondrules and refractory inclusions to reenter the outer regions of the solar nebula at hypersonic speeds (Liffman and Toscano 2000).

The jet model will be used in this paper to investigate the observed size sorting of chondrules and metal grains within the primitive chondritic meteorites.

If one compares the radii a and densities ρ of metal grains

(which we denote by *M*) and silicate chondrules (denoted by *C*), it has been suggested that the equation:

$$\rho_C a_C \approx \rho_M a_M \approx \text{constant} \quad (1)$$

is approximately true for some chondrite classes. That is, silicate chondrules will tend to be larger than metal grains in a ratio that is approximately inversely proportional to their densities. For example, in a preliminary study, Skinner and Leenhouts (1993a) provided observational evidence that this may be true for the CR2 chondrite, Acfer 059. This and related findings have been taken as evidence that the chondrules and metal grains were aerodynamically size-sorted in the solar nebula (Dodd 1976; Kuebler et al. 1999).

WHY THE JET MODEL?

We have assumed the jet flow model of chondrule formation because we wish to examine whether the aforementioned size sorting could have occurred as a consequence of the particles moving in the jet flow or across the face of the solar nebula (Skinner and Leenhouts 1993b).

There are a number of other models in the literature which seek to understand how such size sorting arose. For example, Cuzzi et al. (1996) suggested that turbulence-induced vortices in the solar nebula played a role in the possibly related problem of producing the chondrule size spectrum. Cuzzi et al. proposed that vortices of the appropriate size can selectively sample or filter the original chondrule size spectrum so that the filtered chondrules are concentrated within the vortices which then preferentially form planetesimals. Cuzzi et al. (1999, 2001) were able to theoretically reproduce the chondrule size spectrum after some renormalization of the chondrule size data.

While it is probable that chondrules and other meteoritic components were subject to turbulent gas dynamics in the solar nebula, the Cuzzi et al. analysis raises issues that require further investigation. There is, for example, the problem of what happens to the chondrules or particles outside the size-selection vortices? If planetesimals had traversed a reasonable portion of the solar nebula, they probably would have sampled some of these non-vortex particles. In the meteoritic record, we would expect to see layered samples of the vortex-selected particles and of the non-vortex particles. We do not see such complementary sets of particle distributions within meteorites. The non-vortex particles would probably have had a lower spatial density, but it is still an issue requiring quantitative investigation. Another issue is an apparent incomplete understanding of how the vortices produce size selection. Due to this lack of understanding, Cuzzi et al. are required to renormalize their theoretical results to fit the chondrule size spectrum. This is not an ideal situation; it is preferable to have theory directly replicate observations.

A final but minor issue is that Cuzzi et al. use the standard (but approximate) form of the Epstein drag law to obtain their results. A more exact form is given in Appendix A.

Another size sorting model uses fluidization of materials within an asteroid to separate chondrules and metal grains, e.g., Huang and Sears (1995), Benoit et al. (1998), Ackridge and Sears (1998, 1999). This model has a firm experimental basis. Such metal/rock fractionation is certainly observed in fluidized or vibrated granular material (ibid. and, e.g., Liffman et al. 2001). Unfortunately, there are also problems with this particular model. Granular material can only be fluidized if the cohesive forces between the particles are small compared to the forces of drag and buoyancy. It only takes a minute amount of cohesive material to drastically change the behavior of granular materials (Hornbaker et al. 1997). As such, due to liquid or organic material within the planetesimal, cohesive forces may have destroyed any possibility of fluidization.

Young stellar systems commonly produce bipolar jet flows (Fukui et al. 1993), and these flows eject a considerable mass of material during the lifetime of the system. Although there are significant uncertainties in determining outflow mass loss rates, observations suggest that the total amount ejected for a solar mass ($M_\odot$) star is ~0.1 $M_\odot$ (Hartmann 1998).

A case for the jet model of chondrule formation can be made based on the significant mass of material that may have been processed by an outflow during the lifetime of the solar nebula. For example, it is reasonable to assume that the dust to gas mass ratio of the solar nebula was comparable to the observed interstellar value of ~0.01 (Spitzer 1978). Assuming that the gas ejected by a nebula outflow had a similar solids to gas mass ratio (where it should be noted that a fair portion of the interstellar medium solids may not be metals or silicates), then ~10^{-3}–10^{-4} $M_\odot$ of solid material may have been ejected by the outflow. If 1% of this solid material fell back to the disk (i.e., 10^{-5}–10^{-6} $M_\odot$), it would still have contributed ~1–10% of the total observed or deduced rocky mass of the planets (~10^{-4} $M_\odot$). This simple order of magnitude calculation suggests that a solar jet flow could have recycled a large portion of the solid material in the nebula.

Jet flows are probably produced in a region within ten stellar radii of a star (Hartmann 1992). These inner regions of accretion disks have an abundance of energy available from gravitational accretion—more than enough to make chondrules (Liffman 1992). The subsequent high temperatures of these regions suggest that material may have been heated as it passed through the jet formation region. If this processed material had been ejected to outer, cooler disk regions and subsequently aggregated with the surrounding cooler and (on average) less processed particles, then one would naturally obtain the (carbonaceous) chondrite morphology of "hot" igneous rocks surrounded by "cold" sedimentary matrix. If a solar jet flow reprocessed a large proportion of the solids in the solar nebula, then one should expect to see such material in primitive meteorites.

As with any scientific model, the jet flow model should be judged by what it explains and predicts. The jet model has lead

to a number of explanations as well as predictions, a few of which we shall discuss here. For example, based on mass balance and energetics, Liffman (1992) argued that chondrule formation occurred over a 10^6 to 10^7 yr time scale. This has subsequently been verified (e.g., Russell et al. 2005). Liffman (1992) also argued that chondrules may have been produced by an ablation mechanism where pre-chondrule droplets were produced by the shear interaction between a streaming gas flow and molten material. Kadono and Arakawa (2004) experimentally tested this hypothesis and obtained a size spectrum of droplets that was similar to the chondrule size spectrum. They also obtained a required chondrule formation ram pressure of about 0.1 atm—similar to that given in Liffman (1992). Liffman and Brown (1996) predicted that significant amounts of reprocessed refractory dust would have been formed in the outflow region and spread across the solar nebula. This is consistent with the subsequent observed presence of annealed crystalline dust in comets (Nuth 2001).

The jet model can often provide a tentative explanation where other models may be somewhat less successful. One example is chondrule rim chronology, in which igneous coarse-grained rims (CGRs) are surrounded by fine-grained rims (FGRs), but not the other way around (Grossman et al. 1988).

In the jet model, CGRs are formed at the base of the jet flow in the chondrule formation region, while FGRs are formed when the chondrule rams into the solar nebula (Liffman and Toscano 2000) after the chondrule has been ejected from the jet flow. So, we should expect and see CGRs surrounded by FGRs.

A shock wave can possibly give the sequence of CGR followed by a FGR (Connolly and Love 1998). However, if the first shock wave were later followed by one or more weaker shocks, then one might expect a multi-layer, alternating structure of CGRs and FGRs or a sequence of transition rims on different chondrules where a FGR turns into a CGR. Such rims are not observed.

For the shock model, there is at least one way around this problem: after the rims were formed, the chondrules could have been incorporated into a larger body and thereby protected from further processing. This would be true if the aggregation timescales were much less than the inter-shock timescales. However, if shock waves had a deft enough touch to create/reheat an igneous rim one or more times without remelting the entire chondrule or the prior igneous rim (Kring 1991; Rubin and Krot 1996), it begs the question of why shock waves could not have done the same for fine-grained rims.

As outlined in Liffman and Toscano (2000), our favored scenario is that fine-grained rims formed due to the high speed interaction between the chondrules/CAIs and dust grains. This idea is inspired by experiment. Bunch et al. (1991) showed that supersonic impact of chondrule-sized particles into a low density medium readily forms accretion rims around the particles, and these impact rims shared many of the characteristics seen in fine-grained rims. Some authors (e.g., Cuzzi [2004] and references therein) have shown that the maximum relative velocity between a chondrule and a dust grain (before one has the disruption of dust aggregates on a chondrule surface) is approximately 3 m s^{-1}. Cuzzi (2004) concludes that the high-speed interaction formation scenario for fine-grained rims is simply "not credible." We believe that such a conclusion is premature and is based on an incomplete appreciation of how coatings or rims may be produced.

In the mid 1980s, scientists at the Institute for Theoretical and Applied Mechanics in Novosibirsk, Russia, developed a new coating technology called "cold spray." Using a supersonic jet flow, they accelerated fine, solid powder particles (~1–50 μm in diameter) to speeds between 500 and 1000 m s^{-1}. They found that as the particles rammed into a target surface, they underwent plastic/liquid deformation and rapidly build up a layer of deposited material (Tokarev 1996). Although it is still not clear how such layers form, computer simulations suggest that, as the particles liquify, they interlock and thereby form a tightly bound layer (Grujicic et al. 2003). It is unclear whether a mixture of olivine/metal dust can form fine-grained rim analogues via the cold spray process. We simply point out that the rim formation model of Liffman and Toscano (2000) has, in part, been verified experimentally, but more experimental work is required.

This paper is organized as follows: in the Monte Carlo Simulation section, we show the results from the PROJECTILE Monte Carlo code, which simulates the ejection of chondrule-sized particulate material from a bipolar jet flow. We show that the average physical and elemental structure of the ejecta from the outflow that re-enters the nebula is, in part, dependent on the velocity behavior of the outflow. A more quantitative discussion of relevant aspects of the model is provided in the appendices.

MONTE CARLO SIMULATION

To investigate whether size sorting of the chondrules and metal grains occurred as the particles were moving over or into the solar nebula, we constructed a model solar nebula complete with outflow (Fig. 1).

In this model, it was assumed that the proto-Sun had a mass equal to 1 $M_\odot$ and a radius equal to two solar radii (2 $R_\odot$). The solar nebula accretion disk was modelled using the semi-analytic formula given in Lin (1981). We adopted the Lin model because it was simple to implement and it shows variations in the disk scale height, which allowed us to determine whether such variations altered the fractionation of the particulate ejecta from the outflow that re-enters the solar nebula. This variation in the scale height of the nebula is due to an in-built "snow line," i.e., the distance from the Sun where ice will form. In the Lin model, the position of the snow line is dependent on the mass accretion rate of the disk on to the star. Radiative heating of the disk from the Sun is ignored.

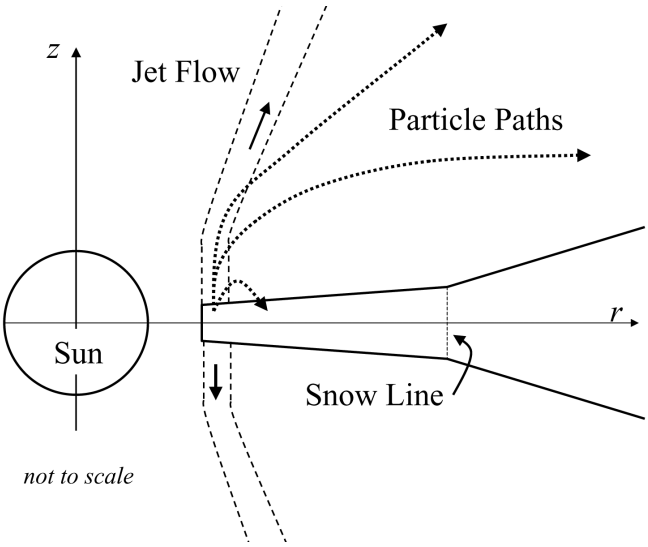

Fig. 1. Schematic depiction of the solar nebula model used in the Monte Carlo simulation. Particles are placed into the base of the outflow and subsequent trajectories are analyzed. The relative sizes of the disk, the Sun, and the outflow are not to scale; r is the distance from the center of the Sun and z is the distance from the midplane of the disk.

For this simulation, we set a disk accretion rate on to the Sun of $\dot{M} = 10^{-8}$ $M_\odot$/year and assumed that the outflow mass loss rate $\dot{M}_o$ was $0.1 \times \dot{M} = 10^{-9}$ $M_\odot$/year, a value consistent with observations. Larger values of the outflow mass loss rate are observed, particularly for very young stellar objects (YSOs), but we chose this smaller value because it is probably closer the solar outflow mass loss rate when chondrules were formed. We also assumed that the accretion disk was approximately isothermal in the z direction, so that the number density $n(r, z)$ of gas particles at a particular distance r from the center of the star and distance z from the disk midplane was:

$$n(r, z) = n(r, 0) \exp\left[-(z/h)^2\right] \quad (2)$$

where h is the isothermal scale height given by:

$$h = \sqrt{\frac{2r^3 k_B T}{\bar{m} G M}} = 0.00253 \left[\frac{\left(\frac{r}{0.07\ \mathrm{AU}}\right)^3 \left(\frac{T}{10^3\ \mathrm{K}}\right)}{\left(\frac{M_*}{M_\odot}\right)\left(\frac{\bar{m}}{m_H}\right)} \right]^{\frac{1}{2}} \mathrm{AU} \quad (3)$$

here T is the temperature of the gas in the disk at a radial distance r from the star, k_B is Boltzmann's constant, $\bar{m}$ the mean molecular mass of the gas, G is the gravitational constant, and M_* is the mass of the central star.

The details of the jet flow model are given in the Magnetic Nozzle and Jet Flow section of Appendix B. Briefly put, we used a magnetic pressure driven (MPD) model developed by the author to power the flow. Most authors use centrifugal wind-driven (CWD) models to understand bipolar jet flow formation, e.g., the X-wind model used in Shu et al. (1996). We have chosen an MPD model, partly because it can provide nearly immediate gas flow acceleration up to the escape speed of the inner solar nebula. Also, MPD devices have been built in laboratories since the late 1950s. So the model does have some experimental validation. There is nothing wrong with the fundamental physics of CWD models, but they tend not have the aforementioned attributes of the MPD model.

Chondrules and metal grains were injected into the outflow at a distance of 0.073 AU from the center of the Sun. This distance was chosen because it is between the inner edge of the disk and the co-rotation radius of solar magnetosphere as given by Equations 59 and 58. If outflows are driven by "wound-up" toroidal magnetic fields, as suggested by the MPD model, then the most probable place for such field formation will be between the inner disk radius and the co-rotation radius.

The initial chondrule and metal grain size spectrum was assumed to be a log normal size distribution (Chondrule and Metal Grain Size Spectrum section of Appendix B). The chondrule and metal grains were given a median diameter D_n of 0.6 mm and 0.26 mm, respectively. The shape parameters σ for both distributions were set to the same value of 0.5. These values are roughly consistent with observations (Dodd 1976). In Fig. 2, we give an example of the initial size distribution of the chondrules and metal grains that were injected into the flow. Each of the chondrules and metal grains had a particular Fe and Si mass abundance (Mass Fractions section of Appendix B) such that the total abundance of Fe and Si was close to solar abundance with a solar atomic abundance Fe/Si ratio of 0.92. The number, type, and size of the particles injected into the flow was set randomly via the standard Monte Carlo method (Sobol 1974), subject to the set constraints of the elemental abundance and size spectrums.

Our computer runs were undertaken by submitting the PROJECTILE Monte Carlo code to the 62 CPU Monash Parallel Parametric Modelling Engine (PPME) or the 192 CPU Victorian Partnership For Advanced Computing (VPAC) linux cluster. The code was shared over the clusters by using the NIMROD/G multiprocessor management system (Abramson et al. 2000). NIMROD/G allowed us to obtain 100% linear scale-up with the multiprocessor systems, i.e., the code ran ten times faster on a ten processor system compared to a one processor system.

The PROJECTILE Monte Carlo code has the capacity to undertake adaptive time steps to minimize run time. However, it turned out that relatively small time steps were required to obtain the appropriate computational accuracy at critical points in the flow. As such, the calculations were much more time-consuming than first expected and it took approximately four months of weekend submissions to generate a million particle paths. The computational methods used to compute the particle paths are discussed in the Mass Fractions section of Appendix B. In the PROJECTILE code, the outflow is

assumed to be produced in a region ranging from the inner radius (Equation 59) to the co-rotation radius (Equation 58) of the disk. The particles were injected into the jet flow at the inner radius at a height of 10^4 km from the midplane of the disk. This height is consistent with the order of magnitude estimate of the "hover height" for a particle in the jet flow as given by Equation 60. The particles were also given a small initial z velocity of 10 m s^{-1} in a direction away from the midplane of the disk.

In Fig. 3, we show the projectile paths of some of the ejected particles as they pass up and through the jet flow and across the surface of the accretion disk. The outline of the disk is shown at one scale height from the midplane of the disk. A particle was deemed to have stopped moving when its radial velocity became very close to zero. At this point, the particle's coordinates and properties were noted for later analysis. It is possible for the code to follow the path of a particle as it subsequently falls toward the midplane of the disk, but in this study we wanted to concentrate on the effect of the radial movement as shown in Fig. 3.

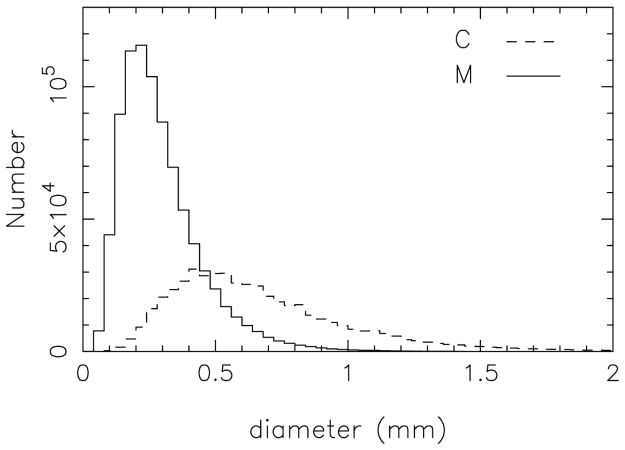

Fig. 2. Initial size spectrum of silicate chondrules (C; broken line) and metal grains (M; unbroken line). In this simulation, 546,640 metal grains and 317,557 chondrules were injected into the flow.

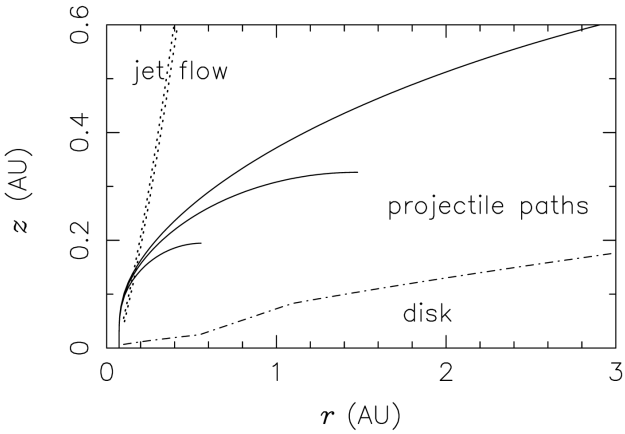

Fig. 3. Examples of projectile paths of chondrules and metal grains ejected from the bipolar outflow.

RESULTS

Bipolar outflows appear to have some variability in their flow speed (e.g., Burrows et al. 1996). If some meteoritic materials were formed in a solar outflow, it is of interest to determine how outflow variability may affect the size and elemental structure of the ejecta that is produced from our model outflow system. As such, we considered two extreme cases: constant flow speed and randomly variable flow speed.

Constant Flow Speed

In this simulation, the maximum flow speed of the jet flow was set to a fixed value of 165 km^{-1}, which was 1.5 times the Keplerian speed at the base of the flow (~110 km s^{-1}). The initial size distribution of the chondrules and metal grains injected into the flow is as shown in Fig. 4a. For this fixed flow speed, it was found that size sorting took place. This can partially be seen in Fig. 4b, which shows the size spectrum of material that was ejected from the solar system (we defined ejected material as chondrules/metal grains that had reached a height of 1.5 AU and/or a radial distance from the Sun greater than 3 AU). There were fairly sharp cut-offs in the chondrule and metal grain sizes at ~0.4 mm and 0.2 mm, respectively. Particles smaller than these sizes were readily ejected from the system. The number and size of particles ejected was dependent on the speed and gas density of the jet flow. It was straight forward to run simulations where larger, more massive particles could be ejected if the jet flows had higher ejection speeds and/or greater gas densities. In this simulation, a fair portion of the larger chondrules and metal grains were stopped at distances less than 0.5 AU from the Sun (Fig. 4c). Comparing Figs. 4b and 4c, it is apparent that shows the size distribution of material that stops between 1.0 and 1.5 AU. Here the size distributions are sharply peaked. There is a clear difference between the size spectrums of Figs. 4a and 4d, and it could be fairly argued that Fig. 4d represents an unrealistic set of size distributions. However, Fig. 4d bears some similarity to the size distributions shown in Skinner and Leenhouts (1993a) for the CR2 meteorite Acfer 059.

We injected 447,276 particles into the base of the outflow of which around 64% of which were metal grains. The Fe/Si ratio of this material was roughly solar ~0.92. There were 128,635 particles ejected 73% of which were metal grains.

The Fe/Si ratio of the ejected material was affected by this greater abundance of metal grains and had a value ~1.82. Most of the material that fell back to the disk landed within 0.5 AU of the Sun and had a total Fe/Si ratio of ~0.89.

The "fallback" behavior can be observed in Fig. 5a, where we plot the proportion of particles (i.e., the number of chondrules divided by the total number of chondrules

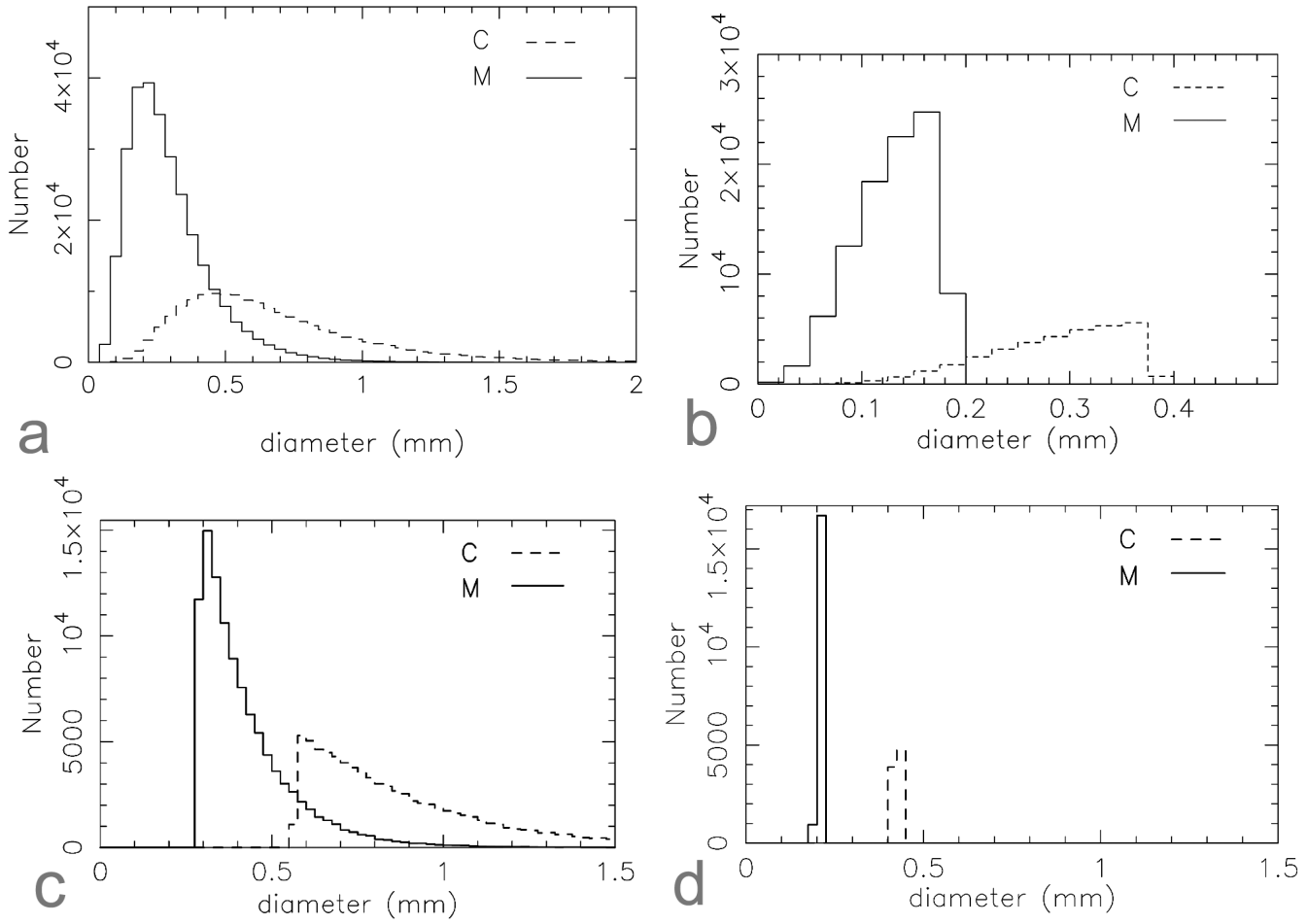

Fig. 4. Chondrule and metal grain size distributions for the constant flow scenario: a) chondrules and metal grains injected into the flow; b) material ejected from the inner region of the solar nebula; c) size distribution of material that stops between 0 and 0.5 AU from the star; d) size distributions of chondrules and grains that stop between 1 and 1.5 AU.

injected into the flow, and similarly with the metal grains) which begin to fallback toward the nebula at a particular radial distance from the Sun. To create this graph, we noted the position of the particles the radial velocity v_r of which became ≤0 and their "vertical" speed $v_z \leq 0$. The number of particles that stopped as a function of r decreased dramatically for $r > 0.5$ AU. We only followed the particle paths to 3 AU, but the number of particles that fell back to the disk clearly decreases as r increases, and we would expect that trend to continue. Another trend for small r is the number of metal grains increases relative to the chondrules, but then the ratio becomes approximately constant (Fig. 5b). At around 0.6 AU, the ratio of the number of metal grains to chondrules exceeds the same ratio of the initial material injected into the outflow.

From Fig. 5c, it is apparent the the absolute sizes of the chondrules and metal grains become approximate constantly for $r > 1$ AU. In Fig. 5d, we plot $\langle a_C \rangle = \langle a_M \rangle$ as a function of r where $\langle a \rangle$ is the average radius. The ratio of these sizes is exactly what would be predicted from size sorting as defined by Equation 1:

$$a_C/a_M \approx \rho_M/\rho_C \quad (4)$$

This size sorted ratio is significantly different from the initial ratio of the particle radii when they were first injected into the jet flow (represented by the dashed line in Fig. 5d). In this way, the jet flow has acted as a particle classifier and has spread size-segregated material across the solar nebula.

As well as these bulk results, the size-sorting was readily observed on an individual scale. We found that one could take a chondrule and a metal grain which satisfied Equation 1 and show computationally that both particles travelled along the same paths if they were placed at the same initial positions in identical flows. This behavior is due to the fundamental structure of the drag force in the particle's equation of motion:

$$\frac{dv_{pi}}{dt} = \frac{-3}{8a_p\rho_p}(\rho_g C_{Dg} + \rho_{sd} C_{Dd}) \quad (5)$$
$$\mathrm{sgn}(v_{pi} - v_{gi})\Sigma_{i=1}^{3}(v_{pi} - v_{gi})^2$$

where v_{pi} and v_{gi} are the components of the particle and gas velocities in the ith direction, respectively, a_p is the radius of

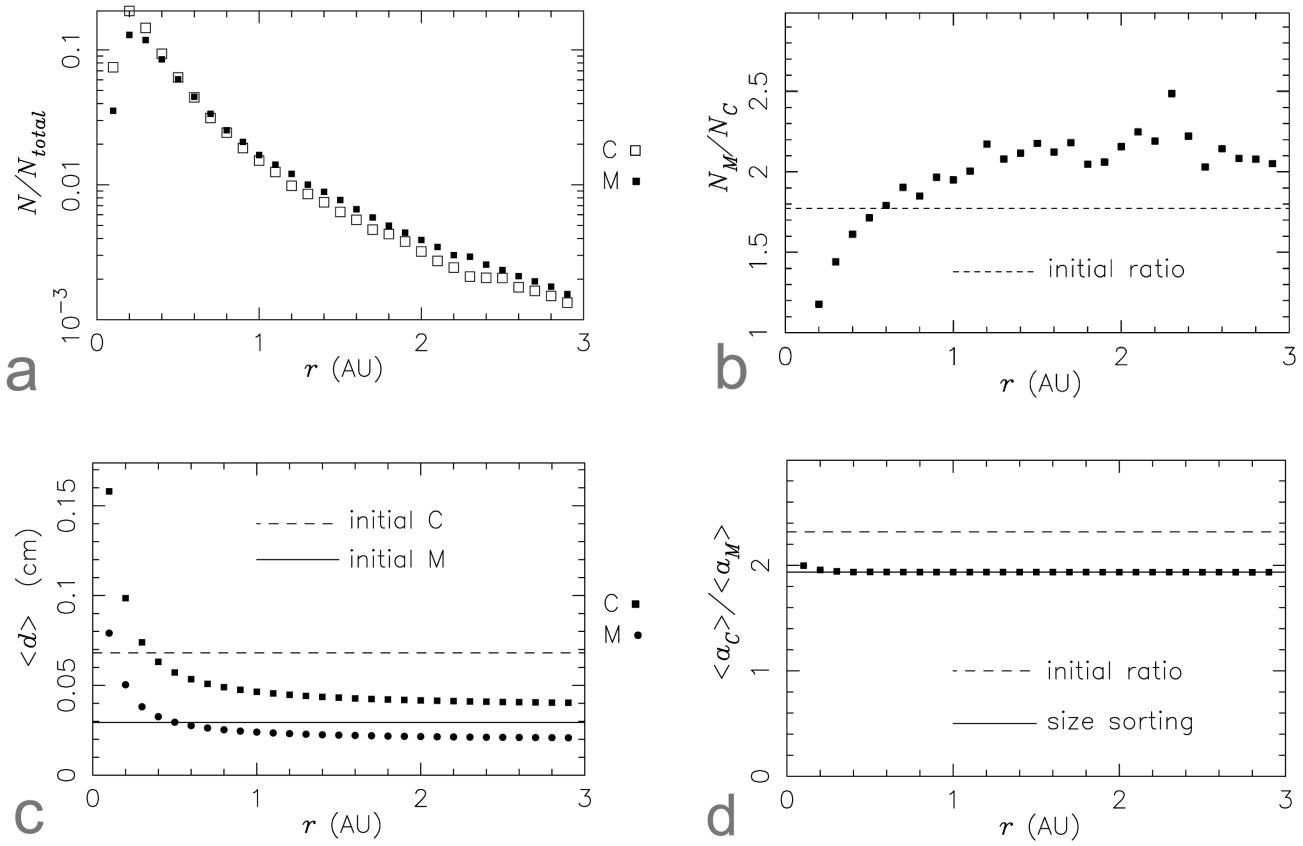

Fig. 5. Physical properties of the material that falls back to the nebular as a function of radial distance r from the Sun: a) proportion of chondrules and metal grains; b) number ratio of metal grains to chondrules; c) absolute diameters; and d) ratio of chondrule to metal grain radii.

the "particle" (i.e., the chondrule or metal grain), ρ_p is the mass density of the particle, ρ_g is the mass density of the gas, $\rho_{sd} = m_d n_d$ is the spatial mass density of the dust (in this paper we set $\rho_{sd} = 0$), C_{Dg} is the drag coefficient between the particle and the gas, C_{Dd} is the drag coefficient between the particle and the dust (the analytic expressions for C_{Dg} and C_{Dd} are given in Liffman and Toscano 2000), and $\text{sgn}(v_{pi} - v_{gi})$ gives the sign of the quantity $(v_{pi} - v_{gi})$. From Equation 5, the drag forces on two different particles are exactly the same provided that the quantity $a_p\rho_p$ is the same for both particles, i.e., provided Equation 1 is satisfied. Thus, any two particles that have the same value of $a_p\rho_p$ will follow exactly the same path provided their launch conditions are identical.

The iron to silicate ratio of the fallback material is given in Fig. 6. Over most of the computed fallback range, the Fe/Si ratio was significantly in excess of the solar value. The Fe/Si ratio was approximately proportional to the ratio of the number of metal grains to silicate chondrules (Fig. 5a). This proportionality arose due to the strong size sorting. This implies that, for a constant jet flow speed, the Fe/Si ratio is dependent on the number of metal grains to chondrules, which in turn is dependent on the initial relative size distributions of metal grains to chondrules.

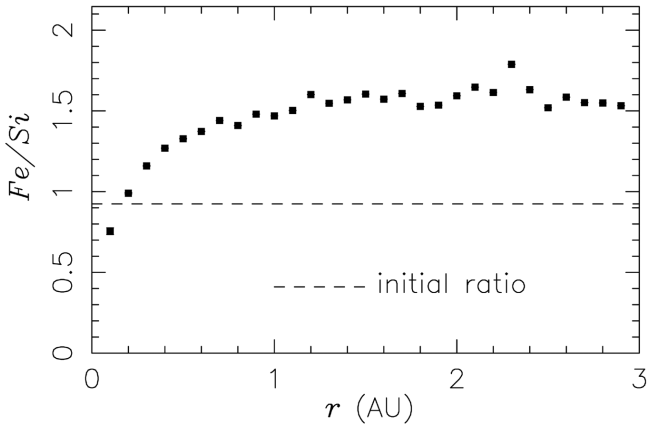

Fig. 6. Iron to silicate ratio of fallback material as a function of distance from the Sun. The line represents the initial solar Fe/Si ratio for the material injected into the outflow.

Variable Flow Speed

For this simulation, we set the outflow to have the final outflow speed in the range of 1 to 2.2 times the Keplerian

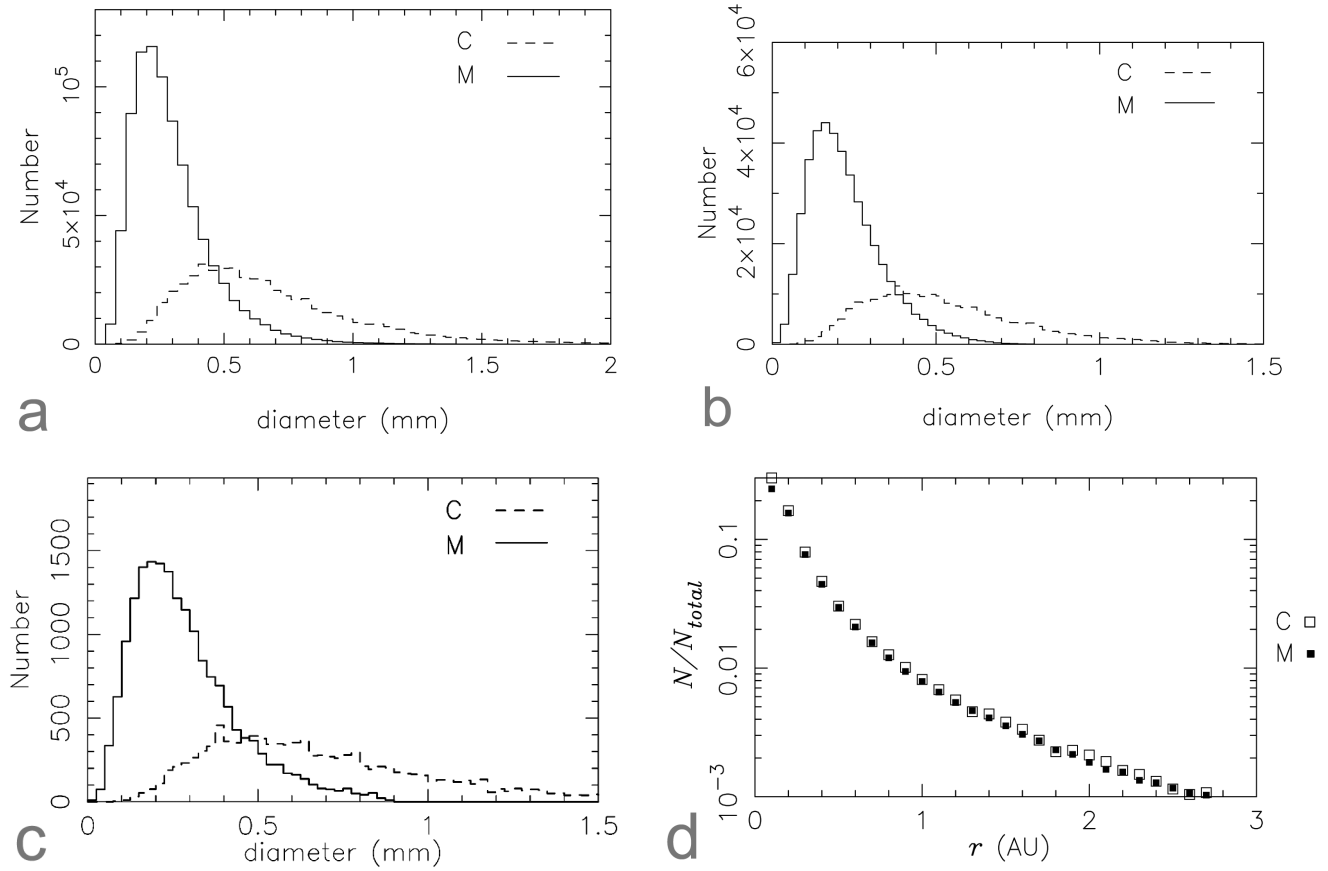

Fig. 7. Chondrule and metal grain size distributions for the variable flow scenario: a) chondrules and metal grains injected into the flow; b) material ejected from the inner region of the solar nebula; c) size distribution of material that stops between 1.0 and 1.5 AU from the star; d) proportion of chondrules and metal grains as a function of distance r from the Sun.

speed at the base of the outflow, i.e., 110 to 240 km s^{-1}. The speed of the outflow for each particle was set randomly. Besides this random variation in outflow speed, there was no difference between the conditions in this simulation and in the previous constant flow speed simulation discussed in the Constant Flow Speed section.

Although size sorting still occurred on an individual particle basis, the random nature of the outflow speed washed out any size sorting behavior. There was very little obvious difference between the size spectra obtained for particles initially injected into the flow (Fig. 7a) relative to material ejected from the flow (Fig. 7b) and the material that began to fallback toward the nebula at a radial distance of 1 to 1.5 AU from the Sun (Fig. 7c). However, there was a difference in the Fe/Si ratios. The initial material had an Fe/Si ratio of ~0.92, ejected material ~1.1, and the fallback material ~0.97.

The proportion of material falling back to the nebula as a function of radial distance from the Sun (Fig. 7d) decreased slightly faster than for the constant flow case (Fig. 5a). Although, the overall shape of the two distributions was quite similar. This suggests that the fallback behavior may be partially due to the geometry of the particle interaction with the nebula as well as the speed of the outflow.

As the simulation progressed, it became clear that the physical characteristics of the fallback material were slowly converging to the characteristics of the chondrules and metal grains that were initially injected into the flow. This can be seen in Figs. 8a–8d. Figures 8a and 8b in particular show the ratios $\langle a_C \rangle / \langle a_M \rangle$ and Fe/Si, respectively. In both cases, the ratios are very close to (or are converging to) the initial values of the materials injected into the flow. The error bars on the values of $\langle a_C \rangle / \langle a_M \rangle$ and Fe/Si increase with increasing r due to relatively small number of particles that fell in these regions.

CONCLUSIONS

We have used a Monte Carlo code to investigate how size sorting of the particulate material in chondritic meteorites may have been produced in the context of the outflow model for chondrule and metal grain formation.

We assumed that a solar bipolar outflow arose from the inner region of the solar nebula due to the interaction between

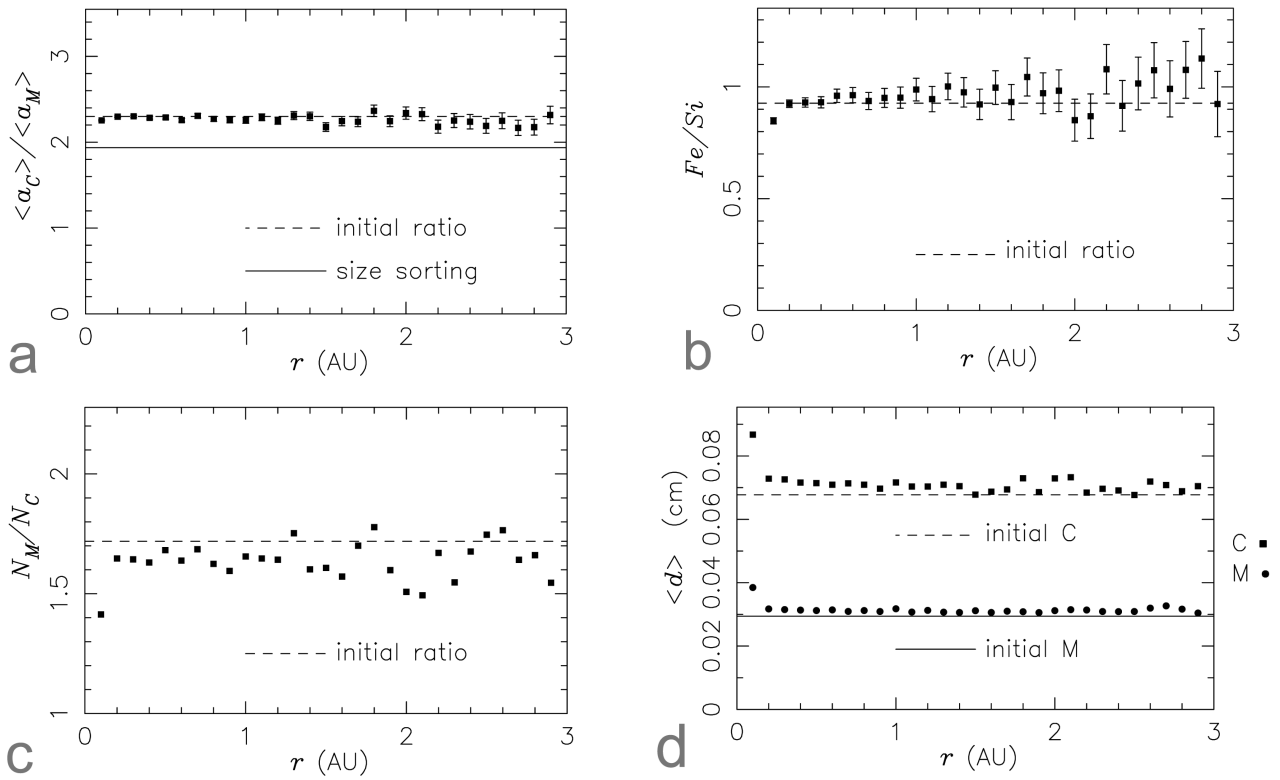

Fig. 8. Physical properties of the material that falls back to the nebula as a function of radial distance r from the Sun: a) ratio of the average metal grain radius to the average chondrule radius; b) average iron to silicate ratio; c) number ratio of metal grains to chondrules; d) absolute diameters.

the Sun's magnetosphere and the most inner regions of the solar nebula. Chondrules and metal grains were injected into the outflow at a specific distance from Sun.

We observed that the number of particles that impact into the nebula drops off moderately rapidly as a function of distance r from the Sun. We suspect that this is partially a geometric effect due to the shape of the nebula, but a more detailed analysis is required to confirm this hypothesis.

Our results suggest that outflows can produce size-sorted material, provided that the solar nebula jet flow has a relatively constant flow rate as function of time. A constant flow rate outflow produces a sharp, size-sorted distribution of particles across the nebula and a metal-rich Fe/Si ratio.

When the other extreme of a fully random flow rate is examined, it is found that size sorting is removed. The outflow distributes material across the nebula with the same size distribution and elemental abundance as the material that is initially injected into the flow. In this way, the outflow acts as a transfer mechanism for material from the inner nebula to the outer nebula without further size sorting or processing. These results indicate that the outflow can act as a size and density classifier. By simply varying the flow rate, the outflow can produce different types of proto-meteorites from the same chondrule and metal grain feed stock. Thus, the outflow model may act as a simple unifying mechanism that can potentially produce the observe meteorite types via a change in one or two parameters.

Acknowledgments–I wish to acknowledge Dr. Brigitte Zanda for her calculations regarding the percentage by mass of Fe and Si in silicate and metal grains. I also wish to thank Colin Enticott from Monash University, who ran the PROJECTILE Monte Carlo code on the Monash University's MC^2 parametric cluster.

Editorial Handling—Dr. Randy Korotev

REFERENCES

Abramson D., Giddy J., and Kotler L. 2000. High-performance parametric modelling with Nimrod/G: Killer application for the global grid? Proceedings, 15th International Parallel and Distributed Processing Symposium. pp. 520–528.

Akridge G. D. and Sears D. W. G. 1998. Chondrule and metal size-sorting in asteroidal regoliths: Experimental results with implications for chondritic meteorites (abstract #1198). 29th Lunar and Planetary Science Conference. CD-ROM.

Akridge G. D. and Sears D. W. G. 1999. The gravitational and aerodynamic sorting of meteoritic chondrules and metal: Experimental results with implications for chondritic meteorites. *Journal of Geophysical Research* 104:11,853–11,864.

Benoit P. H., Akridge G., and Sears D. W. G. 1998. Size sorting of

metal, sulfide, and chondrules in Sharps (H3.4) (abstract #1457). 29th Lunar and Planetary Science Conference. CD-ROM.

Boss A. P. 1996. A concise guide to chondrule formation models. In *Chondrules and the protoplanetary disk,* edited by R. H. Hewins, Jones R. H., and Scott E. R. D. Cambridge: Cambridge University Press. pp. 257–263.

Boss A. P., and Graham J. A. 1993. Clumpy disk accretion and chondrule formation. *Icarus* 106:168–178.

Bunch T. E., Shultz P., Cassen P., Brownlee D., Podolak M., Lissauer J., Reynolds R., and Chang S. 1991. Are some chondrule rims formed by impact processes? Observations and experiments. *Icarus* 91:76–92.

Burrows C. J., Stapelfeldt K. R., Watson A. M., Krist J. E., Ballester G. E., Clarke J. T., Crisp D., Gallagher J. S., III, Griffths R. E., Hester J. J., Hoessel J. G., Holtzman J. A., Mould J. R., Scowen P. A., Trauger J. T., and Westphal J. A. 1996. Hubble Space Telescope observations of the disk and jet of HH 30. *The Astrophysical Journal* 473:437–451.

Cameron A. G. W. 1994. Astrophysical processes contributing to the formation of meteoritic components (abstract). *Meteoritics* 29: 454.

Ciesla F. J. and Hood L. L. 2002. The nebular shock wave model for chondrule formation: Shock processing in a particle-gas suspension. *Icarus* 158:281–293.

Connolly H. C., Jr and Love S. G. 1998. The formation of chondrules: Petrologic tests of the shock wave model. *Science* 280:62–67.

Contopoulos J. 1995. A simple type of magnetically driven jets: An astrophysical plasma gun. *The Astrophysical Journal* 450:616–627.

Cuzzi J. N., Dobrovolskis A. R., and Hogan R. C. 1996. Turbulence, chondrules, and planetesimals. In *Chondrules and the protoplanetary disk,* edited by Hewins R. H., Jones R. H., and Scott E. R. D. Cambridge: Cambridge University Press. pp. 35–44.

Cuzzi J. N., Hogan R. C., and Paque J. M. 1999. Chondrule size-density distributions: Predictions of turbulent concentration and comparison with chondrules disaggregated from L4 ALH 85033 (abstract #1274). 30th Lunar and Planetary Science Conference. CD-ROM.

Cuzzi J. N., Hogan R. C., Paque J. M., and Dobrovolskis A. R. 2001. Size-selective concentration of chondrules and other small particles in protoplanetary nebula turbulence. *The Astrophysical Journal* 546:496–508.

Cuzzi J. N. 2004. Blowing in the wind, III. Accretion of dust rims by chondrule-sized particles in a turbulent protoplanetary nebular. *Icarus* 168:484–497.

Desch S. J. and Connolly H. C., Jr. 2002. Model of the thermal processing of particles in solar nebula shocks: Application to the cooling rates of chondrules. *Meteoritics & Planetary Science* 37: 183–207.

Dodd R. T. 1976. Accretion of the ordinary chondrites. *Earth and Planetary Science Letters* 30:281–291.

Epstein P. S. 1924. On the resistance experienced by spheres in their motion through gases. *Physical Review* 23:710–733.

Fukui Y., Iwata T., Mizuno A., Bally J., and Lane A. P. 1993. Molecular outflows. In *Protostars and planets, III,* edited by Levy E. H. and Lunine J. I. Tucson: The University of Arizona Press. pp. 603–639.

Greenspan D. 1981. *Computer-oriented mathematical physics.* Oxford: Pergamon Press. 170 p.

Grossman J. N. 1988. Formation of chondrules. In *Meteorites and the early solar system,* edited by Kerridge J. F. and Matthews M. S. Tucson: The University of Arizona Press. pp. 680–696.

Grossman J. N., Rubin A. E., Nagahara H., and King A. E. 1988. Properties of chondrules. In *Meteorites and the early solar system,* edited by Kerridge J. F. and Matthews M. S. Tucson: The University of Arizona Press. pp. 619–659.

Grujicic M., Saylor J. R., Beasley D. E., DeRosset W. S., and Helfritch D. 2003. Computational analysis of the interfacial bonding between feed-powder particles and the substrate in the cold-gas dynamic-spray process. *Applied Surface Science* 219: 211–227.

Hartmann L. 1992. Winds from protostellar accretion disks. In *Nonisotropic and variable outflows from stars,* edited by Drissen L., Leitherer C., and Nota A. A.S.P. Conference Series 22. San Francisco: The Astronomical Society of the Pacific, pp. 27–36.

Hartmann L. 1998. *Accretion processes in star formation.* Cambridge: Cambridge University Press. 237 p.

Hayes W. D. and Probstein R. F., 1959. *Hypersonic flow theory.* New York: Academic Press. 464 p.

Hood L. L. 1998. Thermal processing of chondrule precursors in planetesimal bow shocks. *Meteoritics & Planetary Science* 33: 97–107.

Hood L. L. and Horanyi M. 1991. Gas dynamic heating of chondrule precursor grains in the solar nebula. *Icarus* 93:259–269.

Hood L. L. and Horanyi M. 1993. The nebular shock wave model for chondrule formation: One-dimensional calculations. *Icarus* 106: 179–189.

Hornbaker D. J., Albert R., Albert I., Barabasi A. L., and Schiffer P. 1997. What keeps sandcastles standing? *Nature* 387:765.

Huang S. and Sears D. W. G. 1995. Gas flow and fluidization in a thick dynamic regolith: A new mechanism for the formation of chondritic meteorites (abstract). 26th Lunar and Planetary Science Conference. pp. 639–640.

Icke V. 1981. Are bipolar nebulae biconical? *The Astrophysical Journal* 247:152–157.

Kadono T. and Arakawa M. Forthcoming. Breakup of liquids by high velocity flow and size distribution of chondrules. *Icarus.*

Königl A. and Pudritz R. E. 2000. Disk winds and the accretion-outflow connection. In *Protostars and planets IV,* edited by Mannings V., Boss A., and Russell S. Tucson: The University of Arizona Press. pp. 759–788.

Kring D. A. 1991. High-temperature rims around chondrules in primitive chondrites: Evidence for fluctuating conditions in the solar nebula. *Earth and Planetary Science Letters* 105:65–80.

Kuebler K. E., McSween H. Y., Jr., Carlson W. D., and Hirsch D. 1999. Sizes and masses of chondrules and metal-troilite grains in ordinary chondrites: Possible implications for nebular sorting. *Icarus* 141:96–106.

Liffman K. 1992. The formation of chondrules via ablation. *Icarus* 100:608–620.

Liffman K. 1998. An analytic flow solution for YSO jets. *Publications of the Astronomical Society of Australia* 15:259–264.

Liffman K. and Brown M. 1995. The motion and size sorting of particles ejected from a protostellar accretion disk. *Icarus* 116: 275.

Liffman K. and Brown M. J. I. 1996. The protostellar jet model of chondrule formation. In *Chondrules and the protoplanetary disk,* edited by Hewins R. H., Jones R. H., and Scott E. R. D. Cambridge: Cambridge University Press. pp. 285–302.

Liffman K. and Siora A. 1997. Magnetosonic jet flow. *Monthly Notices of the Royal Astronomical Society* 290:629–635.

Liffman K. and Toscano M. 2000. Chondrule fine-grained mantle formation by hypervelocity impact of chondrules with a dusty gas. *Icarus* 143:106–125.

Liffman K., Muniandy K., Rhodes M., Gutteridge D., and Metcalfe G. 2001. A segregation mechanism in a vertically shaken bed. *Granular Matter* 3:205–214.

Lin D. N. C. 1981. Convective accretion disk model for the primordial

solar nebula. *The Astrophysical Journal* 246:972–984.
Nakamura K. E., Nakamura F. E., Fukue J., and Mineshige S. 1995. Winds from the inner region of accretion disks. *Publications of the Astronomical Society of Japan* 47:317–321.
Nuth J. A, III. 2001. How were comets made? *American Scientist* 89: 228–235.
Probstein R. F. 1968. The dusty gas dynamics of comet heads. In *Problems of hydrodynamics and continuum mechanics,* edited by M. A. Lavret'ev. Philadelphia: Society for Industrial and Applied Mathematics. pp. 568–583.
Rubin A. E. and Krot A. N. 1996. Multiple heating of chondrules. In *Chondrules and the protoplanetary disk,* edited by Hewins R. H., Jones R. H., and Scott E. R. D. Cambridge: Cambridge University Press. pp. 173–180.
Russell S. S., Hartman L., Cuzzi J., Krot A. N., Gounelle M., and Weidenshilling S. Forthcoming. Timescales of the solar protoplanetary disk. In *Meteorites and the early solar system II,* edited by Lauretta D., Leshin L. A., and McSween H. Y., Jr. Tucson: The University of Arizona Press.
Ruzmaikina T. V. and Ip W. H. 1996. Chondrule formation in the accretional shock. In *Chondrules and the protoplanetary disk,* edited by Hewins R. H., Jones R. H., and Scott E. R. D. Cambridge: Cambridge University Press. pp. 277–284.
Schoenberg K., Gerwin R., Barnes C., Henins I., Mayo R., Moses R., Jr., Scarberry R., and Wurden G. 1991. *Coaxial plasma thrusters for high specific impulse propulsion.* Reston: American Institute of Aeronautics and Astronautics. 8 p.
Shu F., Shang H., and Lee T. 1996. Towards an astrophysical theory of chondrites. *Science* 271:1545–1551.
Skinner W. R. 1990. Bipolar outflows and a new model for the early solar system. Part II: The origins of chondrules, isotopes, anomalies, and chemical fractionations (abstract). 21st Lunar and Planetary Science Conference. pp. 1168–1169.
Skinner W. R. and Leenhouts J. M. 1993a. Size distributions and aerodynamic equivalence of metal chondrules and silicate chondrules in Acfer 059 (abstract). 24th Lunar and Planetary Science Conference. pp. 1315–1316.
Skinner W. R. and Leenhouts J. M. 1993b. Sorting of chondrules by size and density-evidence for radial transport in the solar nebula (abstract). *Meteoritics* 28:439.
Sobol I. M. 1974, *The Monte Carlo method.* Chicago: The University of Chicago Press. 63 p.
Sorby H. C. 1877. On the structure and origin of meteorites. *Nature* 15:495–498.
Spitzer L. 1978. *Physical processes in the interstellar medium.* New York: John Wiley and Sons. 318 p.
Tokarev A. O. 1996. Structure of aluminium powder coatings prepared by cold gas dynamic spraying. *Metal Science and Heat Treatment* 38:136–139.
Weidenschilling S., Marzari F., and Hood L. L. 1998. The origin of chondrules at jovian resonances. *Science* 279:681–684.
Wood J. A. 1996. Processing of chondritic and planetary material in spiral density waves in the nebula. *Meteoritics & Planetary Science* 31:641–645.

APPENDIX A: EPSTEIN DRAG TIMESCALE

To determine the correct form for the Epstein drag timescale, it is necessary to consider the value of the Knudsen number K_n, which is the ratio of the mean free path of the gas to the radius of the particle r_p.

When $Kn > 10$, we enter the "free molecular flow" regime for gas-particle interactions, where gas atoms/molecules collide with the particle such that interaction with other gas atoms/molecules can be neglected. This is the applicable regime for the projectile motion considered in this paper. So, the appropriate drag coefficient is given by the equation (Probstein 1968; Hayes and Probstein 1959):

$$C_D(s) = \frac{2}{3s}\sqrt{\frac{\pi T_p}{T_g}} + \frac{2s^2+1}{\sqrt{\pi}s^3}\exp(-s^2) + \frac{4s^4+4s^2-1}{2s^4}\,\mathrm{erf}(s) \quad (6)$$

where T_p is the temperature of the particle, T_g is the temperature of the gas, erf(s) the error function, $s\ (= |v_p - v_g|/v_T)$ is the thermal Mach number, with $v_T\ (= \sqrt{2k_B T_g / m_g})$ the thermal gas speed, where v_p is the particle velocity, v_g is the streaming velocity of the gas, m_g the mass of a gas particle and k_B is the Boltzmann's constant.

From Equation 6,

$$s >> 1 \Rightarrow C_D = 2 \quad (7)$$

while

$$s << 1 \Rightarrow C_D = \frac{16}{3\sqrt{\pi}}\frac{1}{s}\left(1 + \frac{\pi}{8}\sqrt{\frac{T_p}{T_g}}\right) = \frac{16}{3\sqrt{\pi}}\frac{1}{s}C \quad (8)$$

here

$$C = \left(1 + \frac{\pi}{8}\sqrt{\frac{T_p}{T_g}}\right) \quad (9)$$

Equation 8 is a more general version of Epstein's famous gas-drag equation (Epstein 1924). In the planetary science literature, C is set equal to 1, which is physically incorrect.

To work out the drag time scale, the relevant equation of motion is:

$$m_p\frac{dv_{pg}}{dt} = -\frac{C_D}{2}A_p\rho_g v_{pg}^2 \quad (10)$$

where m_p is the mass of the particle, A_p is the cross sectional area of the particle, ρ_g the mass density of the gas and $v_{pg} = |v_p - v_g|$.

Assuming spherical particles and Equation 8, Equation 10 has the solution

$$v_{pg}(t) = v_{pg}(0)\exp(-t/\tau) \quad (11)$$

where τ is the Epstein drag timescale:

$$\tau = \frac{\sqrt{\pi}r_p\rho_p}{2Cv_T\rho_g} \quad (12)$$

where here ρ_p is the mass density of the particle. This time

scale differs by the factor $\mathcal{C}$ from the timescale used in the literature.

APPENDIX B: COMPUTATIONAL MODEL

The Magnetic Nozzle and Jet Flow

Our bipolar jet flow is assumed to be powered by a magnetic nozzle. In an astrophysical context, the basic theory of the magnetic nozzle is outlined in Contopoulos (1995) and Liffman and Siora (1997). These magnetic jets are not just theoretical constructs, but have been built in the laboratory, where they have obtained flow speeds of order 100 km s^{-1}.

The magnetic nozzle (also known as the magneto plasmo dynamic or MPD) model is completely different from the standard astrophysical model for bipolar jet flows because it is assumed/deduced that the flows are primarily driven by a strong magnetic field component perpendicular to the flow. Most astrophysical jet flow models assume that the field driving the flow in parallel to the flow (Königl and Pudritz 2000). One can show that such "parallel" flows have a system speed which is the sound speed of the medium. That is why parallel flows require an extra centrifugal component to drive the flow to speeds of astrophysical/astronomical interest.

In contrast, the magnetic nozzle does not require an extra force component to drive flow. The flows are driven to very high speeds purely by the magnetic gradient in the "perpendicular" fields. In such a system the perpendicular magnetic fields tend to "stiffen" the medium, so the nozzle can support flows with speeds of order the fast-magnetosonic speed, C_F ($= \sqrt{[C_S^2 + C_A^2]}$), where C_S is the sound speed and C_A is the Alfvén speed. For a typical parameterization, the sound speed

$$C_S \approx 11.8\left(\frac{T}{10^4 K}\right)^{1/2} \text{km s}^{-1} \tag{13}$$

is usually much less than the Alfvén speed

$$C_A = 282\left(\frac{B}{100 \text{ Gauss}}\right)\left(\frac{10^{-12} \text{ g cm}^{-3}}{\rho}\right)^{1/2} \text{km s}^{-1} \tag{14}$$

and the possibility of high speed flow is apparent.

The flow in the 1D magnetic nozzle is described by the analytic equation (Schoenberg et al. 1991; Liffman 1998):

$$\left(\frac{u}{C_{FT}}\right)\left[\frac{3}{2} - \frac{1}{2}\left(\frac{u}{C_{FT}}\right)^2\right] = \frac{\Delta_T}{\Delta} \tag{15}$$

where u is the flow speed in the nozzle, Δ is the width of the nozzle, C_{FT} and Δ_T are, respectively, the values of C_F and Δ at the throat or narrowest section of the nozzle.

Current theoretical work, developed by the author (to be submitted for publication), suggests that the nozzle is located at the surface of the inner disk. The flow starts with $u \gtrsim 0$ at the start of the nozzle, where the effective Δ is large but $<\infty$. As the flow accelerates, the nozzle converges until the flow reaches the throat, where $u = C_{FT}$. The flow reaches a maximum speed of

$$u_{max} = \sqrt{3} C_{FT} \tag{16}$$

at the exit of the diverging nozzle.

In our Monte Carlo code, we set u_{max} and, therefore, C_{FT}, via the equation

$$u_{max} = V_{Kep}\,[1 + \Psi(\alpha - 1)] \tag{17}$$

where Ψ is a random number between 0 and 1, α is a number >1, and V_{Kep} is the Keplerian speed

$$V_{Kep} = \sqrt{\frac{GM_*}{r}} \tag{18}$$

Every particle had its own unique jet flow that was set randomly by the value of u_{max}. For the simulation discussed in the section Monte Carlo Simulation, V_{Kep} ~115 km^{-1} and $\alpha = 2.2$.

To determine the mass density values of the flow used in Monte Carlo Simulation section, we start with the steady-state continuity equation

$$\nabla \cdot (\rho_g u) = 0 \tag{19}$$

Integrating this equation over the flow domain shown in Fig. 9, we obtain

$$\rho_g u 2\pi r \Delta = \dot{M}_o \tag{20}$$

where $\dot{M}_o$ is the jet flow mass flow rate, r is the radius of the axisymmetric flow at a particular distance z from the central plane of the accretion disk. Equation 20 allows us to compute ρ_g.

At the throat of the nozzle we have

$$\rho_T u_T 2\pi r \Delta_T = \dot{M}_o \tag{21}$$

where the subscripted variables, ρ_T and u_T are the values of ρ_g and u at the throat of the nozzle. The value of Δ_T, the nozzle width at the throat, is a free parameter that is input into the code. In this simulation $\Delta_T = 1.2 \times 10^5$ m. No physical justification exists for this value; it was set by trial and error. In the next iteration of outflow theory development, this free parameter will be removed. The normalized form of Equation 21 is:

$$\left(\frac{\rho_T}{8 \times 10^{-11} \text{ g/cm}^{-3}}\right)\left(\frac{u_T}{200 \text{ km/s}}\right) \left(\frac{r}{0.07 \text{ AU}}\right)\left(\frac{\Delta_T}{120 \text{ km}}\right) = \left(\frac{\dot{M}_o}{10^{-9} M_\odot/\text{yr}}\right) \tag{22}$$

Once the gas flow has been ejected by the nozzle, we calculated the path of the outflow via the methods outlined in Nakamura et al. (1995). This basically means that the gas speed and density were obtained from Equation 20 plus the Bernoulli and specific angular momentum equations given in Nakamura et al. (1995). As is also discussed in Nakamura et al., the value of Δ can be computed from using the (approximate) outflow streamline equation

$$z = r\sqrt{\left(\frac{r}{r_0}\right)^{2/3} - 1} \tag{23}$$

where r_0 is the value of r when $z = 0$. This equation determines the shape of the outflow. It was first derived by Icke (1981).

Chondrule and Metal Grain Size Spectrum

We assumed a lognormal distribution for the initial size spectrum of the chondrules and metal grains that were injected into the outflow. The lognormal distribution function is

$$f(D) = \frac{1}{\sqrt{2\pi}D\ln\sigma}\exp\left\{-\frac{1}{2}\left[\frac{\ln(D/D_n)}{\ln\sigma}\right]^2\right\} \tag{24}$$

where D is the diameter of the particle, D_n is the median particle diameter and σ is the shape parameter. By integrating Equation 24 in the appropriate manner, it is possible to show that the cumulative frequency distribution for all particles with a diameter $D < D_{max}$ has the following form (Equation 25):

$$F(D < D_{max}) = \begin{cases} \frac{1}{2}\left\{1 + \text{erf}\left[\frac{\ln(D_{max}/D_n)}{\sqrt{2}\ln\sigma}\right]\right\} & (D_{max} > D_n) \\ \frac{1}{2} & (D_{max} = D_n) \\ \frac{1}{2}\left\{1 - \text{erf}\left[-\frac{\ln(D_{max}/D_n)}{\sqrt{2}\ln\sigma}\right]\right\} & (D_{max} < D_n) \end{cases}$$

In our Monte Carlo program, we set $F(D < D_{max})$ to a uniformly distributed random number between 0 and 1. We then used the above Equation 25 to solve for D_{max}. This value of D_{max} became the diameter of the particle that was placed into and subsequently ejected from the jet flow. By using the appropriate values for D_n and σ, we can create realistic chondrule and metal grain size spectrums.

Mass Fractions

In the PROJECTILE Monte Carlo code, it was necessary that each metal grain or silicate chondrule was given the appropriate amounts of iron and silicon. To do this, we were required to deduce the average mass fraction of Fe and Si in metal grains and silicate chondrules. As such, we made two assumptions:

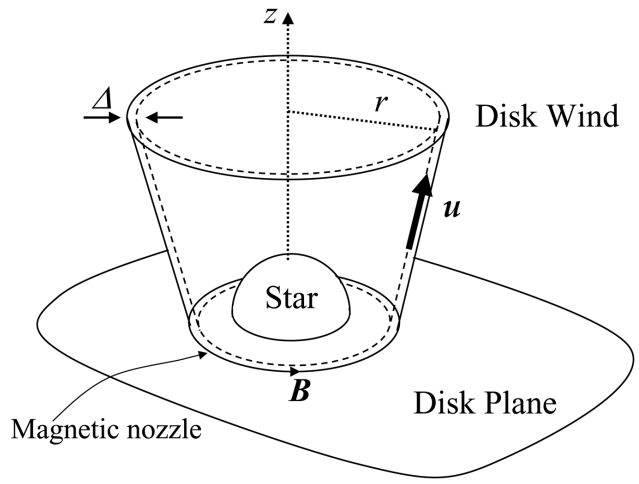

Fig. 9. We consider a thin, axisymmetric element of the flow which arises from a toroidal magnetic field embedded in the accretion disk surrounding a young stellar object (YSO).

1. The protosolar jet pumped out material with standard solar system elemental abundances, and
2. Most of the Fe and Si ended up in silicate chondrules and metal grains.

The rates at which material entered the metal grain (M) and silicate (S) chondrule streams are given by

$$\dot{M}_M = f_M\dot{M}_o \text{ and } \dot{M}_S = f_S\dot{M}_o \tag{26}$$

where $\dot{M}_o$ is the time-averaged rate of mass loss from the protosolar jet, plus f_M and f_S are the mass fractions of $\dot{M}_o$ that enter the S and M streams.

The silicate chondrules contain Si, Fe, and other elements, so the rate at which these elements entered the silicate chondrule stream is

$$\dot{M}_{S_{Si}} = f_{S_{Si}}\dot{M}_S = f_{S_{Si}}f_S\dot{M}_o \tag{27}$$

$$\dot{M}_{S_{Fe}} = f_{S_{Fe}}\dot{M}_S = f_{S_{Fe}}f_S\dot{M}_o \tag{28}$$

and

$$\dot{M}_{S_{other}} = f_{S_{other}}\dot{M}_S = f_{S_{other}}f_S\dot{M}_o \tag{29}$$

By definition

$$1 = f_{S_{Si}} + f_{S_{Fe}} + f_{S_{other}} \tag{30}$$

where f_{S_X} is the average mass proportion of element X that entered into the silicate chondrules. For the metal grain M stream:

$$\dot{M}_{M_{Fe}} = f_{M_{Fe}}\dot{M}_M = f_{M_{Fe}}f_M\dot{M}_o \tag{31}$$

$$\dot{M}_{M_{other}} = f_{M_{other}}\dot{M}_M = f_{M_{other}}f_M\dot{M}_o \quad (32)$$

and

$$1 = f_{M_{Fe}} + f_{M_{other}} \quad (33)$$

where f_{M_X} is the average mass proportion of element X that entered into the metal grains.

If we suppose that all the Si goes into the S stream, then

$$f_{S_{Si}}f_S = a_1 \quad (34)$$

where a_1 is equal to the mass fraction of $\dot{M}_o$ that is composed of Si. From the standard cosmic abundance tables, a_1 = 0.0007672. Let a_2 equal the mass fraction of M_o that is composed of Fe. Then a_2 = 0.001374, and

$$f_{S_{Fe}}f_S + f_{M_{Fe}}f_M = a_2 \quad (35)$$

Fe is contained in both the metal grians and silicate chondrules. Denote the mass fraction of Fe in the metal grains by e. Then

$$f_{M_{Fe}}f_M = e \times a_2 \quad (36)$$

and

$$f_{S_{Fe}}f_S = a_2(1 - e) \quad (37)$$

By comparison with experimental results, our best estimate for the quantity e is $e \approx 0.75$. That is, 75% of the Fe is contained in the metal grains, with the remainder contained in the silicate chondrules. We now need to determine $f_{S_{other}}$ and define the mass fraction a_3 such that

$$f_{S_{other}}f_S = a_3 \quad (38)$$

To find a_3, we note that silicate chondrules are typically composed of olivine [$(Mg, Fe)_2SiO_4$] and pyroxene [$MgSiO_3$, $FeSiO_3$, $CaSiO_3$]. Given this composition, it is possible to construct a chondrule system such that all of the Mg, 35% of the Fe, all of the Si, and at most 20% of the O is tied up in the silicate chondrules. Thus,

a_3 = mass fraction of Mg + 20% mass fraction of O
$= 2.47 \times 10^{-3}$ (39)

Now, from Equations 30, 34, 37, and 38,

$$f_S = a_1 + a_2(1 - e) + a_3 = 3.72 \times 10^{-3} \quad (40)$$

$$f_{S_{Si}} = \frac{a_1}{f_S} = 0.21 \quad (41)$$

$$f_{S_{Fe}} = \frac{a_2(1 - e)}{f_S} = 0.10 \quad (42)$$

and

$$f_{S_{other}} = \frac{a_3}{f_S} = 0.69 \quad (43)$$

So in our model, chondrules are 21% Si and 10% Fe by mass.

We assume that the metal grains are composed of only Fe and Ni. We further assume that all of the Ni is contained in these chondrules. Thus,

$$f_{M_{Fe}}f_M = e \times a_2 \quad (44)$$

and

$$f_{M_{other}}f_M = a_4 \quad (45)$$

As all the Ni is contained in the metal grains, then a_4 = 0.0000792, which is the cosmic mass fraction of Ni. Also,

$$f_{M_{Fe}} + f_{M_{other}} = 1 \quad (46)$$

Therefore,

$$f_M = a_4 + ea_2 = 9.723 \times 10^{-4} \quad (47)$$

and

$$f_{M_{Fe}} \approx 0.93 \quad (48)$$

$$f_{M_{Ni}} \approx 0.07 \quad (49)$$

So the metal grains are assumably 93% Fe and 7% Ni by mass.

Numerics

As shown schematically in Fig. 1, the main function of the PROJECTILE code is to follow the movement of a spherical particle after the particle is placed into the jet flow. Each particle is generated randomly in a manner that is consistent with the Monte Carlo method (Sobol 1974). The size of each particle is determined from a lognormal probability distribution (Chondrule and Metal Grain Size Spectrum section of Appendix B). The density of each particle is determined from mass balance considerations (Mass Fractions section of Appendix B), where we require that the total relative abundances of Fe, and Si are the same as solar abundances.

To determine the path of each particle, the PROJECTILE code integrates the system of equations:

$$\frac{dv_p}{dt} = -\frac{GM_*}{r^2}\frac{r}{|r|} - \frac{3}{8a_p\rho_p}(\rho_g C_{Dg} + \rho_{sd} C_{Dd}) \quad (50)$$
$$(v_p - v_g)^2\frac{(v_p - v_g)}{|v_p - v_g|}$$

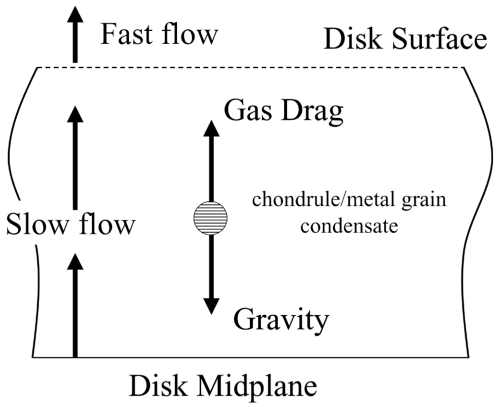

Fig. 10. A particle hovering in the flow.

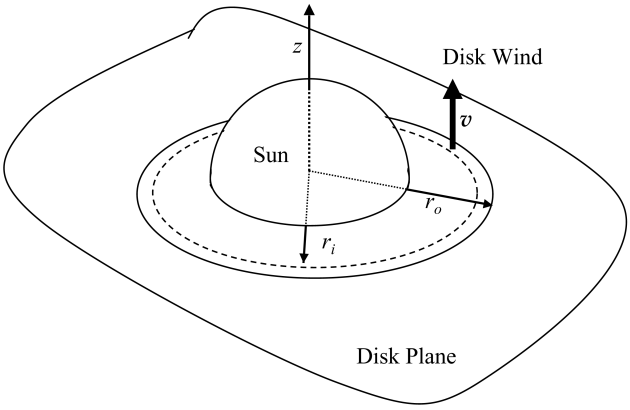

Fig. 11. Disk wind is produced from an annular region of the disk.

The code uses cartesian coordinates so $r = (x, y, z)$, where the origin is located at the center of the Sun; with v_p the velocity of the particle, v_g the gas velocity, G the gravitational constant, and M_* is the mass of the central star. The remaining terms are discussed under Equation 5.

The discretization of the system was obtained from Greenspan (1981) as this discretization is energy conserving. The resulting system of difference equations was integrated by using Newton's method of iteration (ibid.) The accuracy of the code was checked by computing the orbits of particles around the Sun and comparing the orbits with standard analytic solutions. The size of the time steps was determined by computing the particle paths and decreasing the magnitude of the timestep until the solution produced by the code did not change for each progressively smaller timestep.

APPENDIX C: HOVER PARTICLES

Hover Height

Let us consider a particle that has just been created in a jet flow at a position (r, z) from the center of the Sun. As shown in Fig. 10 a particle within the flow will be subject to a gravitational force that is directed toward the midplane of the disk and a drag force due to the streaming gas flow which is directed away from the disk. The particle will probably be accelerated by the jet so that its motion is, initially, in the z direction. The equation of motion for the particle, parallel to the z axis, is given by:

$$m_p\ddot{z} = \frac{C_D}{2}\rho_g(v_{gz}-\dot{z})^2\pi a_p^2 - \frac{GMm_p z}{(z^2+r^2)^{3/2}} \tag{51}$$

where C_D is the coefficient of gas drag, ρ_g the mass density of the gas, v_{gz} the z component of the gas velocity, G the universal gravitational constant, while m_p and a_p are the mass and radius of the particle, respectively.

Suppose the particle reaches a state where the gas drag is balanced by gravity, so that $\ddot{z} = 0$, and $\dot{z} = 0$. Our equation of motion becomes (for $z << r$)

$$0 \approx \frac{C_D}{2}\rho_g v_{gz}^2\pi a_p^2 - \frac{GMm_p z_h}{r^3} \tag{52}$$

where z_h is the value of z for the hovering particle. For z close to the disk midplane, we should expect that a value of z will exist such that v_{gz} will be less than the sound speed, so if the mean free path of the gas l satisfies the relation:

$$\frac{l}{2a_p} \gtrsim 10 \tag{53}$$

then C_D has the form (Appendix A)

$$C_D \approx \frac{(8+\pi)}{3v_{gz}}\sqrt{\frac{8k_B T_g}{\pi m_g}} \tag{54}$$

where k_B is the Boltzmann constant and m_g is the mass of a gas particle.

To obtain a more complete understanding of z_h and the possibility of size sorting in the jet flow, it is useful to consider the jet flow system. We describe our system with cylindrical coordinates, the plane $z = 0$ being the midplane of the accretion disk with the Sun residing at the origin (Fig. 11). In Fig. 11, the jet flow is produced from an annular region within the disk, where r_i is the inner radius of the annulus and r_o is the outer radius. Using Fig. 11, the steady state form of the continuity or mass conservation equation

$$\nabla \cdot (\rho_g v_g) = 0 \tag{55}$$

is readily solved. For an axisymmetric flow, the mass conservation equation has the form

$$2\bar{\rho}_g\bar{v}_{gz}\pi(r_o^2 - r_i^2) = \dot{M}_o \tag{56}$$

where $\bar{\rho}_g$ and $\bar{v}_{gz}(z)$ are the average gas mass-density and jet gas speed, respectively, in the annular jet flow region and M_o is the total mass-loss rate of the outflow. The factor of 2 in Equation 56 arises because the protostellar jet is produced from both sides of the accretion disk.

In Equation 52, ρ_g and v_{gz} are both functions of r. Thus, if

we make the approximation that $\rho_g v_{gz} \approx \bar{\rho}_g \bar{v}_{gz}(z)$ then from Equations 52, 54, and 56 we find that

$$z_h \approx \frac{8+\pi}{16\pi}\left(\frac{8kT_g}{\pi m_g}\right)^{\frac{1}{2}} \frac{\dot{M}r^3}{GM(r_o^2 - r_i^2)a_p\rho_p} \quad (57)$$

One can construct a semi-coherent argument that the jet flow is formed in the region between the inner radius of the disk and the co-rotation radius of the disk. The latter quantity is where the angular frequency of the stellar magnetic field, or at least the plasma attached to the magnetic field, equals the assumed Keplerian angular frequency of the disk. The co-rotation radius is denoted by r_c and is given by the formula:

$$r_o = r_c = \left(\frac{GM}{\Omega_*^2}\right)^{\frac{1}{3}} = 0.078\left[\left(\frac{M}{M_\odot}\right)\left(\frac{P_*}{8 \text{ days}}\right)^2\right]^{\frac{1}{3}} \text{AU} \quad (58)$$

where G is the universal gravitational constant, M is the mass of the Sun, Ω_* is the angular frequency of the proto-Sun, and P_* is the rotational period of the proto-Sun.

We assume that the value of r_i is due to the truncation of the inner disk due to the stellar magnetic field. An approximate expression for r_i can be deduced by equating the gas dynamic and magnetic terms in the magneto-hydrodynamic equation (Equation 59) for the conservation of momentum where μ_0 is the permeability of free space, B_* is the magnitude of the magnetic field strength at the stellar surface, R_* is the stellar radius, and $\dot{M}$ is the disc mass accretion rate.

$$r_i = \left(\frac{4\pi}{\mu_0}\frac{B_*^2 R_*^6}{\dot{M}\sqrt{GM}}\right)^{2/7} = \quad (59)$$

$$0.067\left[\frac{(B_*/0.1\text{T})^2(R_*/2R_\odot)^6}{(\dot{M}/10^{-8}M_\odot \text{ year}^{-1})(M/M_\odot)^{1/2}}\right]^{2/7} \text{AU}$$

Assuming these values for r_i and r_o, we obtain Equation 60, where m_{H_2} is the mass of diatomic hydrogen:

$$z \approx 1.9 \times 10^4 \frac{(\dot{M}/10^{-8}M_\odot/\text{year})(r/r_i)^3(T_g/10^3 \text{ K})^{1/2}}{(m_g/m_{H_2})^{1/2}(M/M_\odot)(\rho_p/5 \text{ gm cm}^{-3})(a_p/0.1 \text{ cm})} \text{ km.}$$